Eighth International Conference on
STEEL AND ALUMINIUM STRUCTURES
Edited by B. Young & Y. Cai
Hong Kong, China, December 7 – 9, 2016

MECHANICS OF DISTORTIONAL-GLOBAL INTERACTION IN FIXED-ENDED LIPPED CHANNEL COLUMNS

André D. MARTINS[1], Dinar CAMOTIM[1], Rodrigo GONÇALVES[2] and Pedro B. DINIS[1]

[1]CERIS, ICIST, DECivil, Instituto Superior Técnico, Universidade de Lisboa, Portugal
[2]CERIS, ICIST and Universidade Nova de Lisboa, Portugal
Emails: andrerdmartins@ist.utl.pt, dcamotim@civil.ist.utl.pt, rodrigo.goncalves@fct.unl.pt, dinis@civil.ist.utl.pt

Keywords: Fixed-ended lipped channel columns; Distortional-Global interaction; Generalized Beam Theory (GBT); Geometrically non-linear imperfect analysis (GNIA).

Abstract. *This work reports the results of a numerical investigation concerning the elastic post-buckling behaviour of fixed-ended thin-walled lipped channel columns affected by distortional-global (D-G) interaction. The columns analysed (i) exhibit cross-section dimensions and lengths ensuring simultaneous distortional and global critical buckling loads, and (ii) contain critical-mode initial geometrical imperfections (linear combinations of D and G buckling modes). For comparison and clarification purposes, the post-buckling behaviour of columns buckling in an "isolated" distortional mode and containing "pure" distortional and global (flexural-torsional) initial geometrical imperfections are also analysed. The results presented and discussed are obtained through geometrically non-linear Generalised Beam Theory (GBT) analyses and provide the evolution, along given equilibrium paths, of the column deformed configuration (expressed in GBT modal form), relevant displacement profiles and modal participation diagrams, making it possible to acquire in-depth knowledge on the column D-G interaction mechanics. Finally, particular attention is paid to interpreting the differences exhibited by the several aforementioned column post-buckling behaviours.*

1 INTRODUCTION

Cold-formed steel (CFS) open-section thin-walled members, namely columns, exhibit geometries (cross-section dimensions and lengths) that often make them highly susceptible to several instabilities involving individual (local, distortional, global – L, D, G) and/or coupled (L-D, L-G, D-G or L-D-G) buckling modes. In fact, the efficient design of such member constitutes a very complex task, since mode interaction phenomena may occur even when the associated critical buckling loadings are significantly apart. Therefore, in order to assess the structural response of such members it does not suffice to acquire in-depth knowledge about their "pure"/individual buckling and post-buckling behaviours. Indeed, it is indispensable to account for the possible occurrence of several mode coupling effects, which may erode, to a smaller or larger amount extent (depending on the slenderness), the member ultimate strength – failing to do it may lead to a high likelihood of reaching unsafe designs.

As far as interaction phenomena involving distortional buckling in CFS columns are concerned (*e.g.*, Camotim & Dinis [1]), most of the existing studies, comprising experimental investigations, numerical simulations and/or design proposals, deal with L-D interaction – it is worth mentioning the works of Kwon & Hancock [2], Young *et al*. [3] and Martins *et al*. [4-6]. However, the amount of research available on D-G interaction is much scarcer. Indeed, to the authors' best knowledge, the works addressing the influence of this coupling phenomenon on the post-buckling behaviour and

ultimate strength of CFS columns consist of (i) experimental investigations on rack-section uprights, with and without holes (Crisan *et al*. [7], Dubina *et al*. [8]), lipped channel columns (Santos *et al*. [9][1]) and, more recently, web-stiffened lipped channel columns (Anbarasu & Murugapandian [10])[2], and (ii) the numerical (shell finite element) investigations on simply supported (locally/globally pinned end cross-sections with and free or prevented warping) and fixed-ended lipped channel columns (Dinis & Camotim [13, 14]), and simply supported and warping-prevented rack-section uprights, with or without holes (Crisan *et al*. [15]). Although all the above studies provided clear evidence of the detrimental influence of D-G interaction on the column strength, an investigation on the mechanics of this coupling phenomenon is still lacking – this work aims at contributing towards filling this gap.

The results presented and discussed in this work are obtained by means geometrically non-linear imperfect analyses (GNIA) based on Generalized Beam Theory (GBT) analysis, a one-dimensional bar theory for prismatic thin-walled members that exhibits the accuracy of shell finite element models and yields clarifying modal solutions that provide in-depth insight on the mechanics of the problem under consideration (*e.g.*, Camotim *et al.* [16]). This feature makes GBT-based GNIA ideally suited to investigate mode interaction problems, which involve deformation of various different natures.

This work addresses the elastic post-buckling behaviour of fixed-ended lipped channel columns undergoing D-G interaction. The columns analysed (i) exhibit cross-section dimensions and lengths ensuring simultaneous distortional and global critical buckling (true D-G interaction), and (ii) contain critical-mode initial geometrical imperfections with amplitude equal to $L/1000$ (L is the column length) – they consist of linear combinations of D and G buckling modes, provided by preliminary GBT buckling analyses. For comparison and clarification purposes, the post-buckling behaviour of columns buckling in an "isolated" distortional mode and containing "pure" distortional and global (flexural-torsional) initial geometrical imperfections are also analysed. The GBT-based GNIA results, which are validated through the comparison with values yielded by ABAQUS [17] shell finite element analyses (SFEA), provide the evolution, along given equilibrium paths, of the column deformed configuration (expressed in GBT modal form), relevant displacement profiles and stress distributions, making it possible to acquire in-depth knowledge on the column D-G interaction mechanics. Finally, particular attention is devoted to interpreting the differences exhibited by the several aforementioned column post-buckling behaviours.

2 REVIEW OF THE GBT GEOMETRICALLY NON-LINEAR FORMULATION

The performance of a GBT structural analysis involves two (independent) main tasks, namely (i) a cross-section analysis, leading to the determination of the deformation modes and evaluation of the corresponding modal mechanical properties, and (ii) a member analysis (elastic buckling and post-buckling analyses, in this case). The geometrically non-linear GBT formulation recently developed by the authors (Martins *et al*. [18]) is reviewed next, after which a description of the deformations modes most relevant to the analysis of the lipped channel columns undergoing D-G interaction is provided.

2.1 Formulation, finite element approximation and solution procedure

The member mid-surface displacement field is expressed as products of two one-dimensional functions, namely (i) the deformation mode shapes ($u_k(s)$, $v_k(s)$ and/or $w_k(s)$ – obtained from the cross-section analysis, briefly discussed in Section 2.2) and (ii) the modal amplitude functions $\phi_k(x)$, which constitute the member analysis unknowns. One then has

$$u(x,s) = u_k(s)\phi_{k,x}(x) \qquad v(x,s) = v_k(s)\phi_k(x) \qquad w(x,s) = w_k(s)\phi_k(x) \tag{1}$$

[1] The aim of this work was investigating L-D-G interaction in fixed-ended lipped channel columns. However, it was later concluded that full fixity of the specimen end cross-sections had not been achieved, leading to column failures in D-G interactive modes.

[2] It is still worth noting the tests reported by the Rossi *et al*. [11, 12] on cold-formed stainless steel lipped channel columns.

where (i) $(.)_{,x} \equiv d(.)/dx$ and (ii) Einstein's summation convention applies to subscript k – the initial geometrical imperfections incorporated in the analyses follow the same trends. The kinematic (strain-displacement) relationships adopted are similar to those considered by Gonçalves & Camotim [19] and Kwon & Hancock [20] (GBT and finite strip non-linear analyses, respectively) and read

$$\varepsilon_{xx} = u_{,x} - zw_{,xx} + \frac{1}{2}\left(u_{,x}^2 + v_{,x}^2 + w_{,x}^2\right) - \bar{u}_{,x} + z\bar{w}_{,xx} - \frac{1}{2}\left(\bar{u}_{,x}^2 + \bar{v}_{,x}^2 + \bar{w}_{,x}^2\right) \tag{2.1}$$

$$\varepsilon_{ss} = v_{,s} - zw_{,ss} + \frac{1}{2}\left(u_{,s}^2 + v_{,s}^2 + w_{,s}^2\right) - \bar{v}_{,s} + z\bar{w}_{,ss} - \frac{1}{2}\left(\bar{u}_{,s}^2 + \bar{v}_{,s}^2 + \bar{w}_{,s}^2\right) \tag{2.2}$$

$$\gamma_{xs} = u_{,s} + v_{,x} - 2zw_{,xs} + u_{,x}u_{,s} + v_{,x}v_{,s} + w_{,x}w_{,s} - \bar{u}_{,s} - \bar{v}_{,x} + 2z\bar{w}_{,xs} - \bar{u}_{,x}\bar{u}_{,s} - \bar{v}_{,x}\bar{v}_{,s} - \bar{w}_{,x}\bar{w}_{,s} \tag{2.3}$$

The member strain energy, expressed in terms of the strain and stress components, is given by

$$U = \frac{1}{2}\int_V \sigma_{ij}\varepsilon_{ij}dV = U_1 + U_2 + U_3 - \left(\bar{U}_1 + \bar{U}_2 + \bar{U}_3\right) \tag{3}$$

where U_i and $\bar{U}_i$ $(i = 1,2,3)$ are the strain energy terms associated with the total deformation and initial geometric imperfections, respectively (see the details in [18]).

The modal amplitude functions appearing in (3) are approximated through 4-node beam finite elements based on approximation functions that are linear combinations of:

(i) Lagrange cubic polynomial primitives $\psi_i^L(\xi), i = 1,...,4$, for the (warping only) axial extension and shear modes, which read ($d_{k1} = \phi_{k,x}(0), d_{k2} = \phi_{k,x}(L_e/3), d_{k3} = \phi_{k,x}(2L_e/3), d_{k4} = \phi_{k,x}(L_e)$)

$$\phi_{j,x}(x) = \psi_{1,x}^L d_{j1} + \psi_{2,x}^L d_{j2} + \psi_{3,x}^L d_{j3} + \psi_{4,x}^L d_{j4} \tag{4.1}$$

(ii) Hermite cubic polynomials $\psi_i^H(\xi), i = 1,...,4$, for the remaining (conventional and transverse extension) deformation modes[3], given by ($d_{k1} = \phi_{k,x}(0), d_{k2} = \phi_k(0), d_{k3} = \phi_{k,x}(L_e), d_{k4} = \phi_k(L_e)$)

$$\phi_k(x) = \psi_1^H d_{k1} + \psi_2^H d_{k2} + \psi_3^H d_{k3} + \psi_4^H d_{k4} \tag{4.2}$$

The component of the finite element internal force vector concerning deformation mode h and dof α ($f_{h\alpha}^e$) is obtained by incorporating (4.1)-(4.2) into the strain energy (3) and differentiating with respect to $d_{h\alpha}$, to obtain

$$f_{h\alpha}^e = \frac{\partial U}{\partial d_{h\alpha}} = f_{h\alpha}^1 + f_{h\alpha}^2 + f_{h\alpha}^3 - \left(\bar{f}_{h\alpha}^1 + \bar{f}_{h\alpha}^2 + \bar{f}_{h\alpha}^3\right) \tag{5.1}$$

where, after some manipulation,

$$f_{h\alpha}^1 = T_{hi\alpha\beta}^1 d_{i\beta} \tag{5.2}$$

$$f_{h\alpha}^2 = \frac{1}{2}T_{hi\alpha\beta}^2 d_{i\beta} \tag{5.3}$$

$$f_{h\alpha}^3 = \frac{1}{3}T_{hi\alpha\beta}^3 d_{i\beta} \tag{5.4}$$

$$\bar{f}_{h\alpha}^1 = T_{hi\alpha\beta}^1 \bar{d}_{i\beta} \tag{5.5}$$

$$\begin{aligned}\bar{f}_{h\alpha}^2 = \bar{T}_{hi\alpha\beta}^2 d_{i\beta} + \Bigg(&\frac{1}{2}C_{hij}^I k_{\alpha\beta\eta}^{211} + \frac{1}{2}B_{hij}^I k_{\alpha\beta\eta}^{000} + D_{hij}^I k_{\alpha\beta\eta}^{110} + \frac{1}{2}E_{hij}^I k_{\alpha\beta\eta}^{200} + \frac{1}{2}\left(E_{hij}^{II} + B_{hij}^{II}\right)k_{\alpha\beta\eta}^{011} + \\ &+ \frac{1}{2}C_{hij}^{II} k_{\alpha\beta\eta}^{222} + D_{hij}^{II} k_{\alpha\beta\eta}^{121} + \frac{1}{2}E_{hij}^{III} k_{\alpha\beta\eta}^{022} + \frac{1}{2}E_{ijh}^{IV} k_{\beta\eta\alpha}^{112}\Bigg)\bar{d}_{i\beta}\bar{d}_{j\eta}\end{aligned} \tag{5.6}$$

[3] The various deformation mode families are addressed in Section 2.2.

$$\overline{f}^{3}_{h\alpha} = \overline{T}^{3}_{hi\alpha\beta} d_{i\beta} \tag{5.7}$$

and

(i) $T^{1}_{hi\alpha\beta}, T^{2}_{hi\alpha\beta}, T^{3}_{hi\alpha\beta}, \overline{T}^{2}_{hi\alpha\beta}, \overline{T}^{3}_{hi\alpha\beta}$ are the components of the tangent stiffness matrix (details in [18]) – the elementary tangent stiffness matrix components are given by $\left(\overline{T}^{1}_{hi\alpha\beta} = 0\right)$

$$T^{e}_{hi\alpha\beta} = T^{1}_{hi\alpha\beta} + T^{2}_{hi\alpha\beta} + T^{3}_{hi\alpha\beta} - \left(\overline{T}^{2}_{hi\alpha\beta} + \overline{T}^{3}_{hi\alpha\beta}\right) \tag{6}$$

(ii) $C^{I}_{hij}, C^{II}_{hij}, B^{I}_{hij}, B^{II}_{hij}, D^{I}_{hij}, D^{II}_{hij}, E^{I}_{hij}, E^{II}_{hij}, E^{III}_{hij}, E^{IV}_{hij}$ are third-order tensors concerning the geometrically non-linear behaviour – the second and four-order tensors are also necessary to evaluate the components of the tangent stiffness matrix defined in the previous item [18].

(iii) The reduced stiffness terms $k^{abc}_{\alpha\beta\eta}$ are defined by

$$k^{abc}_{\alpha\beta\eta} = \int_{Le} \frac{\partial^{a}\psi_{\alpha}}{\partial x^{a}} \frac{\partial^{b}\psi_{\beta}}{\partial x^{b}} \frac{\partial^{c}\psi_{\eta}}{\partial x^{c}} dx \tag{7}$$

i.e., another expression involving the product of shape functions and/or derivatives is required to evaluate the components of the tangent stiffness matrix defined in item (i).

The incremental-iterative procedure employed is based on (i) Newton-Raphson's method and (ii) a load or arc-length control strategy (*e.g.*, Crisfield [21] or Ritto-Corrêa & Camotim [22]) – both strategies were implemented and it is worth noting that (i) vector components $\overline{f}^{1}_{h\alpha}$ and $\overline{f}^{2}_{h\alpha}$ depend on the initial geometrical imperfection (see eq. (5.6)) and (ii) the tangent stiffness components $T^{1}_{hi\alpha\beta}, \overline{T}^{2}_{hi\alpha\beta}$ and $\overline{T}^{3}_{hi\alpha\beta}$ are constant and, thus, need to be evaluated only once (before the incremental-iterative procedure). The numerical integration is performed (i) analytically through the thickness (along *z*) and (ii) using the Legendre-Gauss Quadrature with three-point integration along *x* and *y*.

2.2 Cross-section analysis

The GBT cross-section analysis involves a lengthy set of fairly complex operations which has been reported in the literature[4] and the most recent developments can be found in the works of Gonçalves *et al.* [23] and Bebiano *et al.* [24] – the latter provides the fundamentals of the procedure implemented in version 2.0 of code GBTUL (Bebiano *et al.* [25]). The deformation modes are divided into three main sets/families: (i) conventional (or Vlasov), (ii) shear and (iii) transverse extensions (TE) deformation modes. As far as the TE deformation modes are concerned, they can still be divided into linear and quadratic – the latter, not addressed in the above references, play a pivotal role in post-buckling analyses, since they make it possible to capture the Poisson effects, thus precluding overly stiff solutions (Gonçalves & Camotim [19]). The quadratic TE deformations modes are defined, in each wall segment *i*, by $\overline{v}_i(\xi) = \xi b_i^2(\xi - 1)$ and are null in all remaining wall segments ($j \neq i$) – b_i and $\xi = y / b_i$ denote the wall segment width and a normalised coordinate along it.

Figure 1 shows the GBT nodal discretisation adopted in this work, which involves 15 nodes (6 natural and 9 intermediate – 3 per flange and 3 in the web), and leads to (i) 17 conventional modes (4 global, 2 distortional and 11 local – modes **1-17** in Fig. 1), (ii) 14 shear modes (5 global and 9 local – modes **18-31** in Fig. 1), (iii) 14 linear transverse extension modes (1 global isotropic, 4 global deviatoric and 9 local – modes **32-45** in Fig. 1) and (iv) 14 quadratic transverse extension modes (modes **46-59** in Fig. 1), totalling 59 (sequentially numbered) deformation modes.

BUCKLING ANALYSIS – COLUM GEOMETRY/LENGTH SELECTION

The investigation on the mechanics of D-G interaction in lipped channel columns starts with the selection of a geometry (cross-section dimensions and length) prone to this coupling phenomenon,

[4] The interested reader is referred to the bibliography of the GBT research group at the University of Lisbon (*www.civil.ist.utl.pt*).

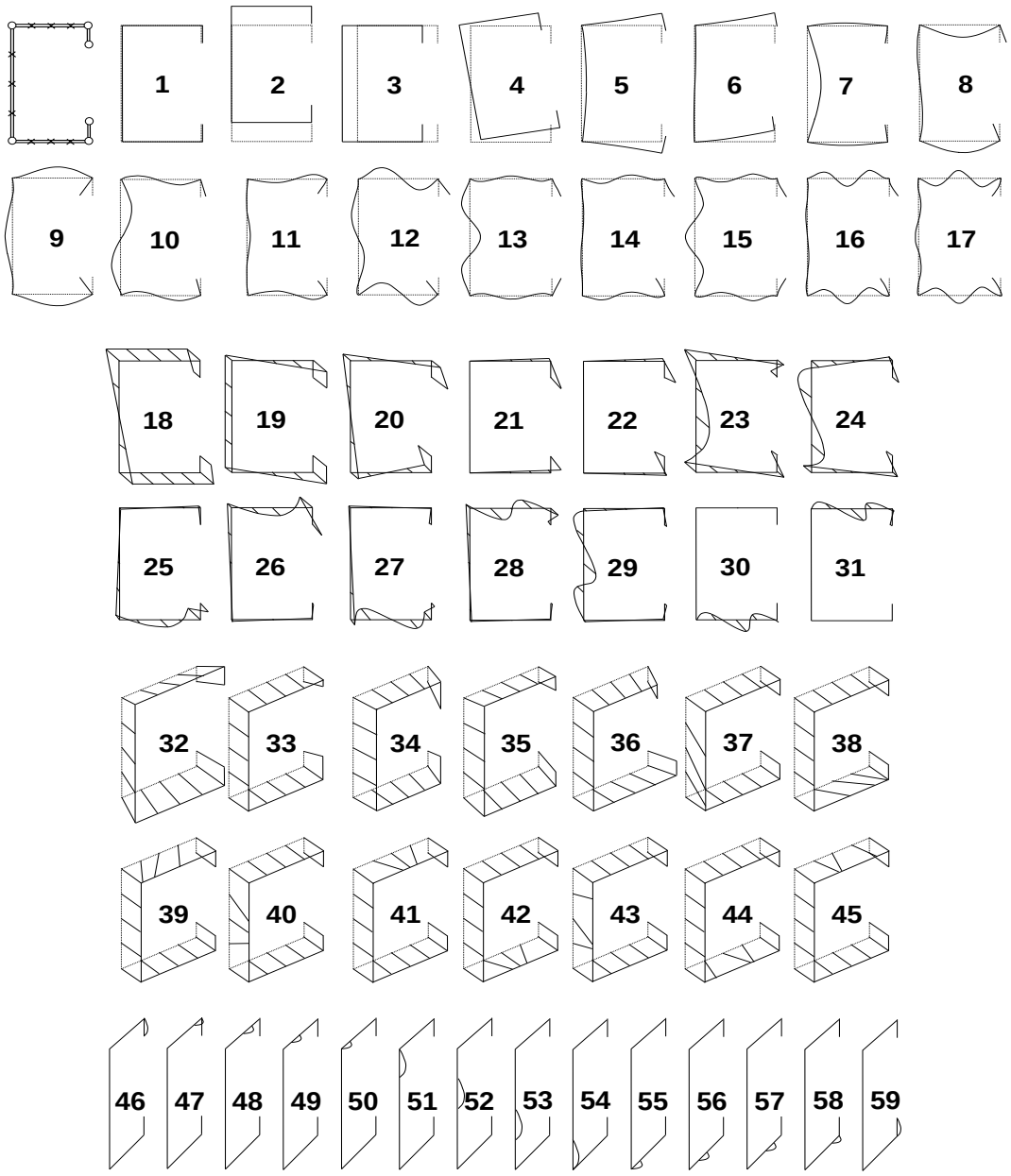

Figure 1: Lipped channel (i) GBT discretisation, (ii) conventional and transverse extension (linear and quadratic) mode in-plane configurations and (iii) shear mode warping displacement profiles

i.e., such that the distortional (P_{crD}) and global (P_{crG}) critical buckling loads are as close as possible. The selection procedure is straightforward, as it is just necessary (i) to find cross-section dimensions such that P_{crD} is significantly lower than its local counterpart (P_{crL}) and (ii) select the intermediate-to-long length associated with the transition from distortional to global critical buckling in the P_{cr} vs. L curve. In order to illustrate this procedure, Fig. 2(a) depicts this curve (L in logarithmic scale), obtained from GBT buckling analyses (E=210GPa, ν=0.3) carried out in GBTUL 2.0 [25] for column cross-section dimensions b_w=10cm b_f=9cm, b_l=1.5cm, t=0.5cm (web-flange-lip widths and wall thickness) – the fairly large wall thickness was adopted to increase the local critical buckling load, thus avoiding the occurrence of L-D-G interaction. Also displayed in Fig. 2(a) is the GBT modal participation diagram, providing the contribution of each deformation mode to the column critical global buckling modes. The observation of these buckling results prompts the following remarks:

(i) The L=155cm column exhibits practically coincident P_{crD}=1273.7kN and P_{crG}=1268.6kN values, which means that its post-buckling behaviour (and strength) is certainly affected by strong D-G

interaction – Fig. 2(a) also shows the two competing buckling mode shapes, which exhibit 4 distortional and 1 global[5] half-waves, respectively.

(ii) The GBT modal participations depicted in Fig. 2(a) show that the P_{cr} vs. L descending branch involves two distinct buckling behaviours[6]. The first involves contributions from deformation modes **2**+**4**+**6**, *i.e.*, the column buckles into a combination of major-axis flexure, torsion and asymmetric distortion (FTD) for $155 < L < 250$cm[7]. In view of the presence of mode **6**, the designation "global" is no longer strictly correct – however, for the sake of simplicity, it will continue to be used in this work (sometimes between quotation marks, if confusion may arise). The longer columns ($250 < L < 1000$cm) buckle in the (expected) flexural-torsional (FT) modes, combining deformation modes **2** and **4** – truly global buckling. Note that the participation of mode **6** gradually decreases with L up to 250cm, when FTD buckling switches to FT buckling.

Fig. 2(b) shows again the P_{cr} vs. L curve depicted in Fig. 2(a), where a column length corresponding to a "pure" distortional buckling and post-buckling behaviour (no interaction occurs) is indicated – L=60cm, associated with a two half-wave buckling mode. The behaviour of this column will play an important role in clarifying some results presented in Section 4. The distortional critical buckling load is much lower than its local and "global" counterparts: P_{crD}=1159.2 <P_{crL}=3643.8 <P_{crG}=7929.9kN).

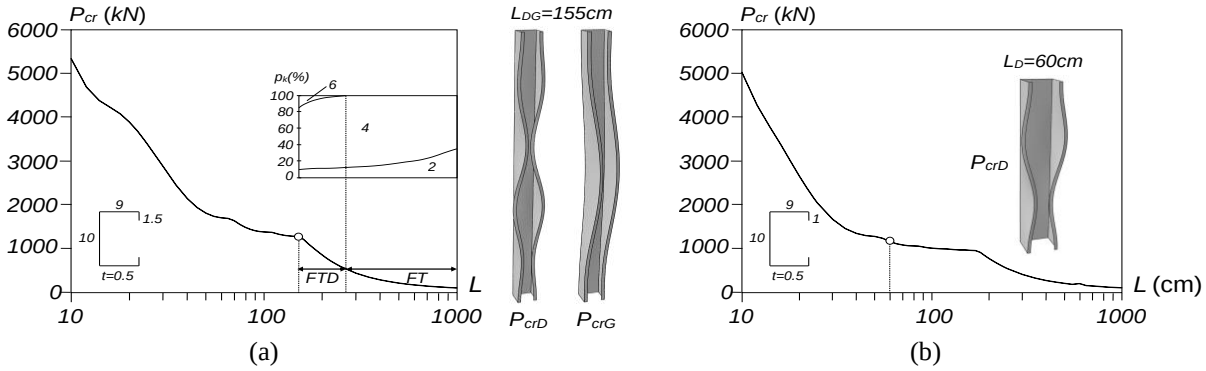

Figure 2: P_{cr} vs. L curves, selected lengths and critical mode shapes of fixed-ended lipped channel columns undergoing (a) distortional-global interaction and (b) distortional buckling

4 COLUMN POST-BUCKLING BEHAVIOUR UNDER D-G INTERACTION

4.1 Validation of the GBT results

This section presents and discusses the validation of the GBT GNIA results of columns under "true D-G interaction", through their comparison with ABAQUS SFEA values. The three columns analysed have the cross-section dimensions selected in Section 3 and length L=1550mm. They differ in the initial geometrical imperfection shape, which is either (i) "global" (FTD) with 1 half-wave and amplitude L/1000, (ii) distortional with 4 half-waves and amplitude L/1000, or (iii) half the sum of the two previous ones – here termed "C_{DG}+G", "C_{DG}+D" and "C_{DG}+{0.5G+0.5D}" column, respectively.

Figs. 3(a)-(c) show the three lipped channel column equilibrium paths P/P_{cr} vs. $(v+v_0)/t$, where v is the flange-lip corner vertical displacement caused by the applied load P, *i.e.*, excluding the initial value, occurring at either mid-span (Figs. 3(a) and 3(c)) or the location of the buckling mode most inward half-wave crest (Fig. 3(b). The initial geometrical imperfection shapes considered are also displayed in Figs. 3(a)-(c) and the equilibrium paths were determined by means of an arc-length control strategy. In order to assess the relevance of the different deformation mode families to the

[5] In addition, there are inflexion points in the close vicinity of the end cross-sections, which define short "quarter-waves" – recall that the columns analysed have fixed end supports. In this work, the half-wave numbers mentioned always exclude these "quarter waves".

[6] Similar conclusions were reported in [13,14].

[7] Note that, while modes **2** and **4** exhibit single half-wave amplitude functions, the mode **6** amplitude function has 3 half-waves.

column post-buckling behaviour, two "approximate analyses" were performed, including the most relevant (i) conventional and linear transverse extension modes (**1-17**+**32-45**), and (ii) conventional, shear and linear transverse extension modes (**1-45**) – the column was axially discretised into 8 finite elements. In addition, analyses including all modes (**1-59**) and with discretisations into 8 and 20 finite elements were also performed. The observation of the above results prompts the following remarks:

(i) The GBT equilibrium paths obtained with deformation modes **1-17**+**32-45** and **1-45** provide accurate results only up to fairly early loading stages. As shown in [18, 19], only the inclusion of the quadratic transverse extension modes (**46-59** – see Fig. 1) makes it possible to replicate the "exact" ABAQUS SFEA solution, by eliminating the membrane locking effects. It is worth noting that, since the column deformation is not symmetric (as will be shown later), more deformation modes need to be included in the analyses than in similar previous studies dealing with column L-D interaction[8] – the exception is the C_{DG}+D column (also addressed latter).

(ii) Since there is virtually no difference between the solutions obtained with 8 and 20 finite elements, it may be concluded that the adoption of the cross-section discretisation shown in Fig. 1 and 8 finite elements leads to very accurate (virtually "exact") results. Thus, only GBT buckling and post-buckling results obtained with such cross-section and longitudinal discretisations are presented and discussed here, in the context of the study of D-G interaction in lipped channel columns.

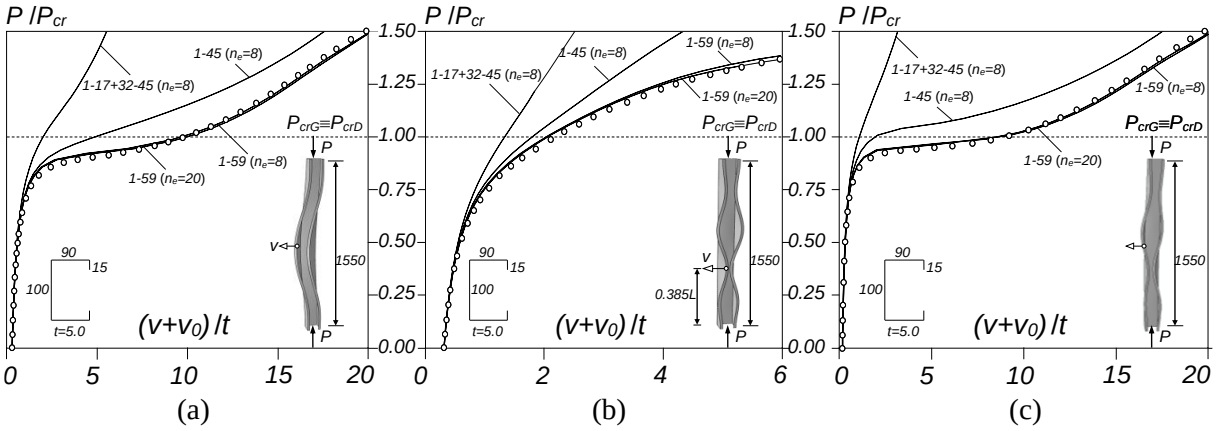

Figure 3: GBT P/P_{cr} vs. $(v+v_0)/t$ paths of lipped channel columns undergoing "true D-G interaction" with (a) "global", (b) distortional and (c) combined "global"-distortional initial geometrical imperfections

4.2 Distortional-global interaction

Figs. 4(a)-(b) show the column equilibrium paths P/P_{cr} vs. $(w+w_0)/t$ and P/P_{cr} vs. $\beta+\beta_0$, where w and β are the mid-span mid-web transverse displacement and web chord rigid-body rotation due to the applied load P – the curves labelled D, G and 0.5D+0.5G concern the C_{DG}+D, C_{DG}+G and C_{DG}+{0.5G+0.5D} columns, respectively[9]. These equilibrium path pairs were chosen to assess the column (i) distortion (through w, not influenced by the torsional mode **4**) and (ii) torsional rotation (through β, not influenced by the deformations caused by the distortional modes **5**+**6**). Moreover, the above figures also display a few illustrative mid-span cross-section deformed configurations. The comparative analysis of these post-buckling results prompts the following remarks:

(i) Generally speaking, the C_{DG}+G and C_{DG}+{0.5G+0.5D} columns exhibit similar post-buckling equilibrium paths (behaviours) – see Figs. 4(a)-(b). Moreover, the two paths merge into a common curve at the advanced post-buckling stages. The fact that both columns experience significant distortional deformations (Fig. 4(a)) and rigid-body rotations (Fig. 4(b)) means that fairly strong D-G interaction is taking place.

[8] The numbers of deformation modes that had to be considered are similar to those involved in the analysis of beams [18].

[9] Figs. 4(a)-(b) also show C_{DG}+{0.95G+0.05D} column equilibrium paths, which will be adressed later.

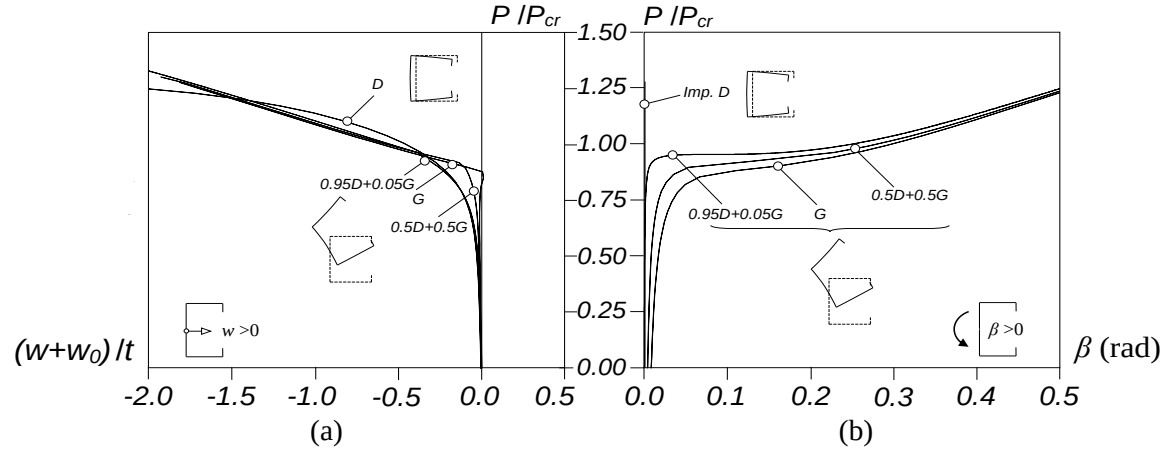

Figure 4: (a) P/P_{cr} vs. $(w+w_0)/t$ and (b) P/P_{cr} vs. $(\beta+\beta_0)$ post-buckling equilibrium paths of columns containing several initial geometrical imperfections

(ii) Hovewer, the post-buckling behaviour of the C_{DG}+D column is completely different: (ii_1) the P/P_{cr} vs. $(w+w_0)/t$ path does not merge with its C_{DG}+G and C_{DG}+{0.5G+0.5D} counterparts and (ii_2) there is a complete absence of rigid-body rotations (Fig. 4(b)). Thus, D-G interaction does not occur and the behaviour appears to be pure distortional. This surprising behavioural feature was first reported in [13, 14] and termed "a different type of D-G interaction". Special attention is devoted here to this column, in order to clarify its post-buckling behaviour – GBT, rather than the SFEA employed in [13, 14], is ideally suited for this task.

(iii) Regardeless of the imperfection type/shape, the column exhibits significant post-critical strength – much higher than the simply supported column affected by D-G interaction that was analysed in [13]. Obviously, these columns also exhibit a much higher post-critical strength than those experiencing a "pure global" post-buckling behaviour.

In order to shed fresh light on the mechanics of the above three columns, (i) modal participation diagrams, (ii) column deformed configurations and (iii) modal displacements profiles are presented and discussed in the remainder of the paper. The modal participation factors can be evaluated on the basis of several criteria, involving specific displacements (*e.g.*, [26]), the strain energy (*e.g.*, [25]) or the modal amplitude functions (*e.g.*, [27]). This work adopts the last criterion, which was found to describe more adequately the behaviour of the columns analysed. The participation of a given deformation mode k in the columns deformed configuration, termed p_k, is given by either

$$p_k = \frac{\int_L \left|\hat{\phi}_k(x)\right| dx}{\sum_{j=1}^{N \le N_T} \int_L \left|\hat{\phi}_j(x)\right| dx} \qquad \text{or} \qquad p_k = \frac{\int_L \left|\hat{\phi}_{k,x}(x)\right| dx}{\sum_{j=1}^{N \le N_T} \int_L \left|\hat{\phi}_{j,x}(x)\right| dx} \qquad (8.1)\text{-}(8.2)$$

depending on the nature of the deformation mode k. Eq. (8.1) is used to determine the participation factors of the conventional (excluding axial extension) and transverse extension deformation modes. Eq. (8.2), on the other hand, is employed for the participation factors of the axial extension and shear modes, *i.e.*, those involving only warping displacements. In these equations, (i) N is the number of deformation modes included in the analysis, (ii) $\hat{\phi}_k(x) = \phi_k(x) - \bar{\phi}_k(x)$ and (iii) N_T is the total number of deformation modes obtained from the cross-section analysis (for a given discretisation). However, the main drawback of the above criterion is the dependence on the deformation mode normalisation. In order to overcome this drawback, the following normalisation is adopted: unit (i) translation for the axial extension and major/minor-axis bending modes, (ii) maximum in-plane displacement ($max\left\{\sqrt{v^2+w^2}\right\}=1$) for the torsion[10] and distortional modes, (iii) maximum transverse displacement

[10] The associated rotation varies with the cross-section dimensions. A unit rotation (1 radian) is inappropriate – very large displacements.

($max\{w\}=1$) for the local modes, (iv) maximum warping displacement ($max\{u\}=1$) for the shear modes and (v) transverse extension ($v_{,s}$=1) for the transverse extension modes.

4.2.1 Columns C_{DG}+G and C_{DG}+{0.5G+0.5D}

Since columns C_{DG}+G and C_{DG}+{0.5G+0.5D} exhibit similar post-buckling behaviours (see Fig. 4), the corresponding results are presented and discussed jointly. Figs. 5(a)-(b), 6(a_1)-(b_5), 7(a)-(n) and 8(a)-(n) show, for both columns, the (i) modal participation diagrams, providing the evolution of the relative contributions of the various deformation modes to the column deformed configuration, (ii) deformed configurations at five loading stages (P/P_{cr}=0.50-0.75-1.00-1.25-1.50 – amplifications given inside brackets) and (iii) the evolution of the top/bottom flange-lip corner vertical displacement profiles (v_2^{top}, v_4^{top}, v_5^{top}, v_6^{top}, $v_{32\text{-}45}^{top}$, $v_{1\text{-}59}^{top}\equiv v^{top}$, v_5^{bot}, $v_{32\text{-}45}^{bot}$ and $v_{1\text{-}59}^{bot}\equiv v^{bot}$ – note that the contributions from modes **3**, **7-17** and **46-59** are null) and mid-web transverse displacement profiles (w_3, w_5, $w_{7\text{-}17}$, $w_{32\text{-}45}$ and $w_{1\text{-}59}\equiv w$), caused by various deformation modes or mode sets. The observation of all these post-buckling results leads to the following conclusions:

(i) The comparison of the two modal participation diagrams shown in Fig. 5(a)-(b) shows that the major differences between the two column deformed configurations occur mostly for P/P_{cr}<1.00. Indeed, besides the equally predominant contribution from mode **1**, there are differences between columns C_{DG}+G and C_{DG}+{0.5G+0.5D} concerning the remaining modal contributions. For instance, at P/P_{cr}=0.50 one has: mode **2** (4% vs. 2%), mode **4** (36% vs. 18%) mode **5** (0% vs. 21%) and mode **6** (7% vs. 4%). These differences reflect the distinct initial geometrical imperfection shapes. As loading progresses, the mode **1** participation is gradually decreases (from 65% to 50%)and is replaced by increases in the remaining mode contributions, with one exception: mode **2**, whose contribution remains practically unaltered (in both columns).

(ii) In column C_{DG}+G (see Fig. 5(a)), mode **5** appears at $P/P_{cr}\approx$0.75 and its participation rises quickly from 2% to 11% at $P/P_{cr}\approx$0.90 – for P/P_{cr}>0.90, p_5 starts to decrease slowly and smoothly. As for mode **3**, it emerges at the peak of p_5 (P/P_{cr}=0.90) and becomes progressively more relevant: p_3 grows from 2% at $P/P_{cr}\approx$0.90 to 14% at P/P_{cr}=1.50, which stems from increasing effective centroid shift effects (stress redistribution caused by the increasing distortional deformations).

(iii) In column C_{DG}+{0.5G+0.5D} (see Fig. 5(b)), on the other hand, p_5 reaches a peak value of 28% at $P/P_{cr}\approx$0.87 and then decreases continuously until 7% at P/P_{cr}=1.50. Conversely, p_3, which emerges again at the peak of p_5, increases quickly from 3% to 14%.

(iv) The evolutions of the remaining modal participations are quite similar in both columns. First of all, mode **4** dominates the column response (see also Fig. 6): its participation reaches 57% at $P/P_{cr}\approx$1.05 and then decreases very slowly to 55% at P/P_{cr}=1.50 (due to the p_3 increase). As for mode **6**, its participation reaches a peak of 11% (9%) at $P/P_{cr}\approx$0.90 (0.97) and decreases

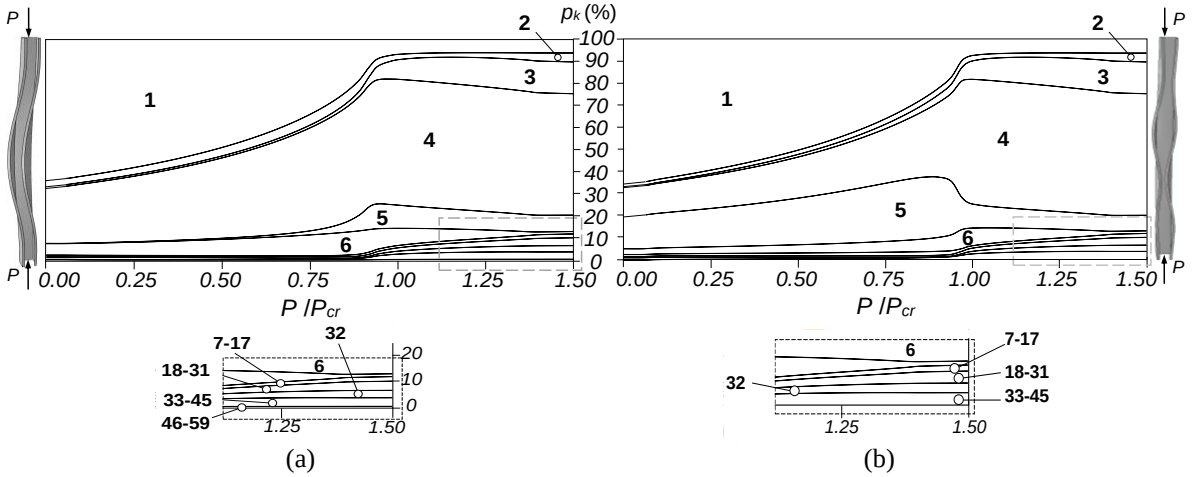

(a) (b)

Figure 5: Modal participation diagrams for columns (a) C_{DG}+G and (b) C_{DG}+{0.5G+0.5D}

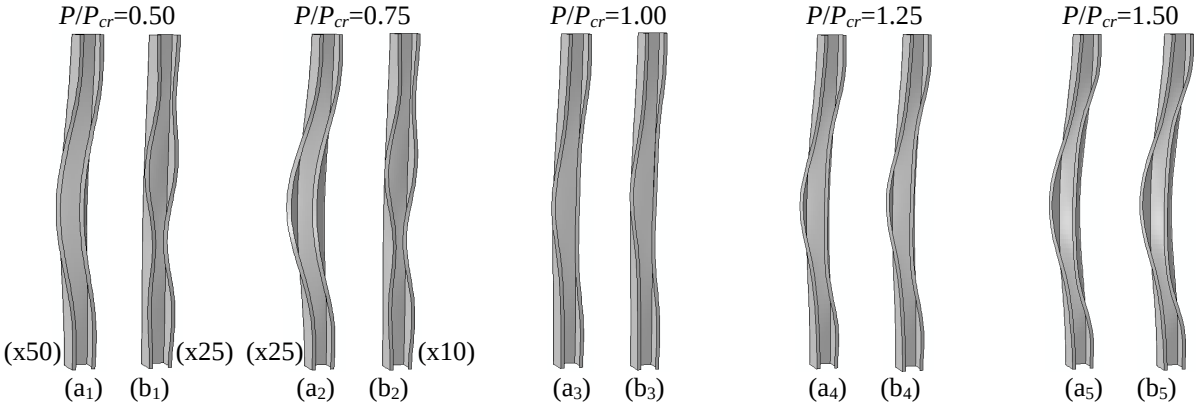

Figure 6: ABAQUS deformed configurations of columns (a) C_{DG}+G and (b) C_{DG}+{0.5G+0.5D} columns at the loading stages defined by P/P_{cr} equal to ($_1$) 0.50, ($_2$) 0.75, ($_3$) 1.00, ($_4$) 1.25 and ($_5$) 1.50

drastically to 1% at P/P_{cr}=1.50. The joint participation of the local modes (mostly mode **7**) never exceeds 2% and the shear modes only emerge at $P/P_{cr}\approx$0.90, with a joint participation (modes **18**, **19** and **20** – mostly mode **19**) that never exceeds 4%. Finally, even if the joint participation of the transverse extension modes only becomes visible for P/P_{cr}>0.90 and reaches a maximum of 6%, it should be noted that mode **32** is present since the early loading stages and its inclusion in the analysis is essential to obtain accurate results, even if p_{32} only varies between 1% and 3% – the remaining 3% are due to modes **33** (0.7%), **34** (0.2%), **35** (0.2%), **36** (0.8%) and **37** (0.9%).

(v) In the C_{DG}+G column, the displacement profiles due to the contributions of modes **2** and **4** (see Figs. 7(a)-(b)) retain more or less their initial shapes (one half-wave – "better shaped" in the case of mode **4**) as loading progresses – they practically coincide with v^{top} and v^{bot} at the early loading stages (see Figs. 7(f)+(i))[11]. Likewise, the v_5^{top} and v_5^{bot} displacement profiles, which only become visible at P/P_{cr}=0.818, retain their 5 half-wave shape (akin to the second distortional buckling mode – see the configurations at P/P_{cr}=0.818 in Figs. 7(c)+(g). This apparently surprising emergence of distortional deformations akin to the second distortional bucking mode (instead of the critical one, which has 4 half-waves – see Fig. 2(a)), is due to the (v_1) near coincidence of the buckling loads associated with the first two distortional buckling modes (1273kN vs. 1281kN) and (ii_2) shared axial symmetry of the second distortional and critical "global" buckling modes, which favours the interaction between them. Indeed, Fig. 7(a_3), concerning P/P_{cr}=1.00, provides clear evidence of the occurrence of D-G interaction, combining distortional and global deformations – symmetric and anti-symmetric with respect to the the major-axis, respectively. The presence, since the early loading stages, of deformation patterns akin to the distortional and global buckling modes characterises the so-called "true D-G interaction"[12].

(vi) Since the C_{DG}+{0.5G+0.5D} column contains initial geometrical imperfections that combine "global" (modes **2**+**4**+**6**) and distortional (mode **5**) components, exhibiting 1 and 4 half-waves[13], respectively, the qualitative changes observed in the evolution of the displacement profiles shown in Figs. 8(a)-(n) are more significant than those occurring in their C_{DG}+G column counterparts, displayed in Figs. 7(a)-(n). For instance, Figs. 8(c)+(g) clearly show that, for P/P_{cr}>0.904, the

[11] The displacement profile due to the contribution of mode **6** (see Fig. 7(d)) changes gradually from 3 half-waves (akin to its component in the initial geometrical imperfections) to 7 half-waves between P/P_{cr}=0.818 (when mode **5** emerges) and P/P_{cr}=1.424 – the mechanics behind this behavioural feature change are not yet well understood, particularly because mode **6** does not participate in the distortional buckling modes. Nevertheless, it should be also mentioned that the above change is accompanied by a decrease in relevance of mode **6**, as far as the column deformed configuration is concerned.

[12] Columns with global-to-distortional critical buckling load ratios higher than 1.00 (distortional buckling precedes global buckling) may also experience D-G interaction, termed "secondary distortional-bifurcation D-G interaction" – however, this type of D-G interaction is not addressed here. Conversely, columns with global-to-distortional critical buckling load ratios lower than 1.0 are not expected to undergo D-G interaction, due to the minute column global post-critical strength reserve.

[13] Recall that the mode **6** amplitude function exhibits 3 half-waves.

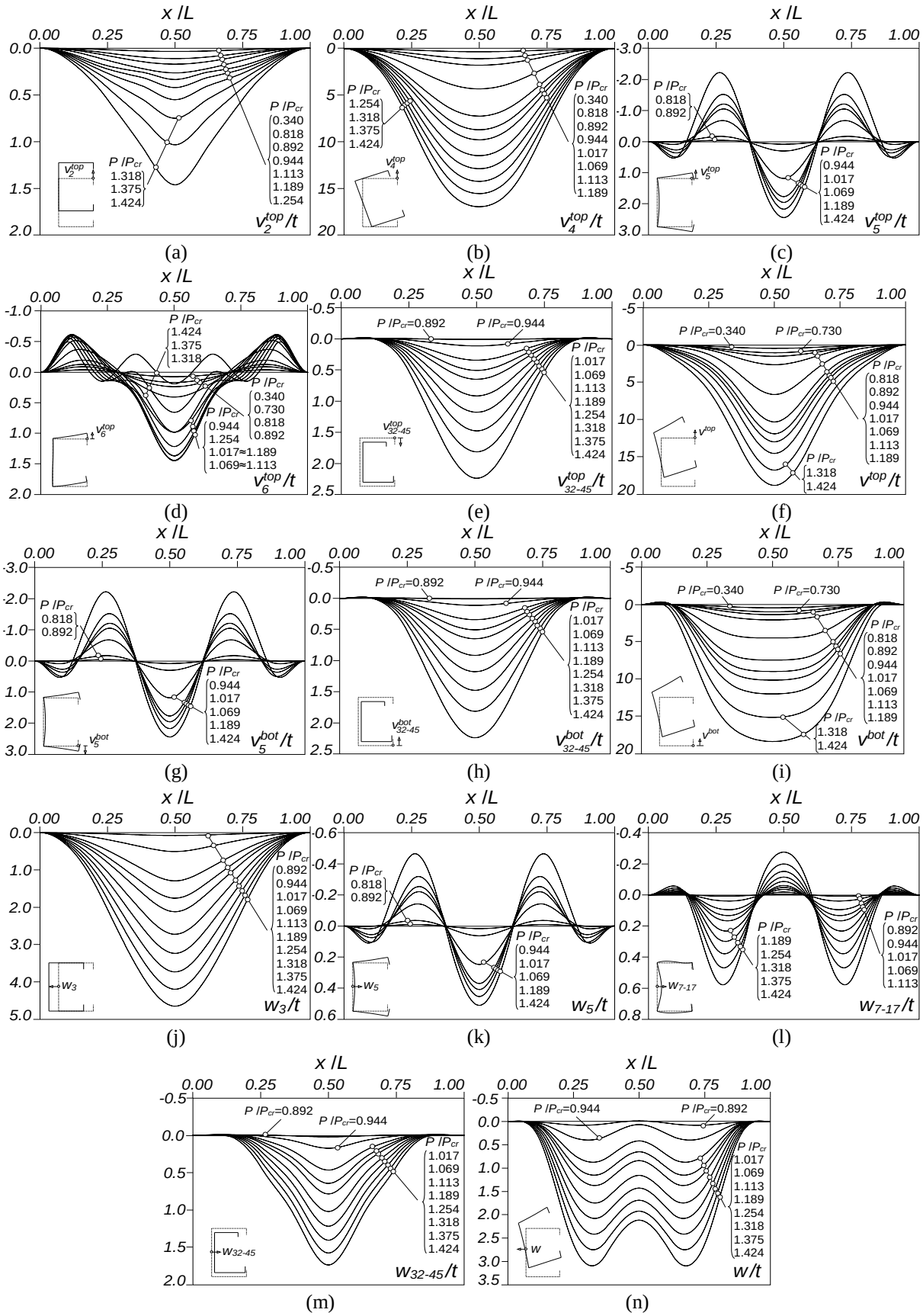

Figure 7: C_{DG}+G column displacement profiles: top flange-lip corner vertical displacement (a) v_2^{top}, (b) v_4^{top}, (c) v_5^{top}, (d) v_6^{top}, (e) $v_{32\text{-}45}^{top}$, (f) $v_{1\text{-}59}^{top} \equiv v^{top}$, bottom flange-lip corner vertical displacement (g) v_5^{bot}, (h) $v_{32\text{-}45}^{bot}$, (i) $v_{1\text{-}59}^{bot} \equiv v^{bot}$ and mid-web transverse displacement (j) w_3, (k) w_5, (l) $w_{7\text{-}17}$, (m) $w_{32\text{-}45}$, and (n) $w_{1\text{-}59} \equiv w$

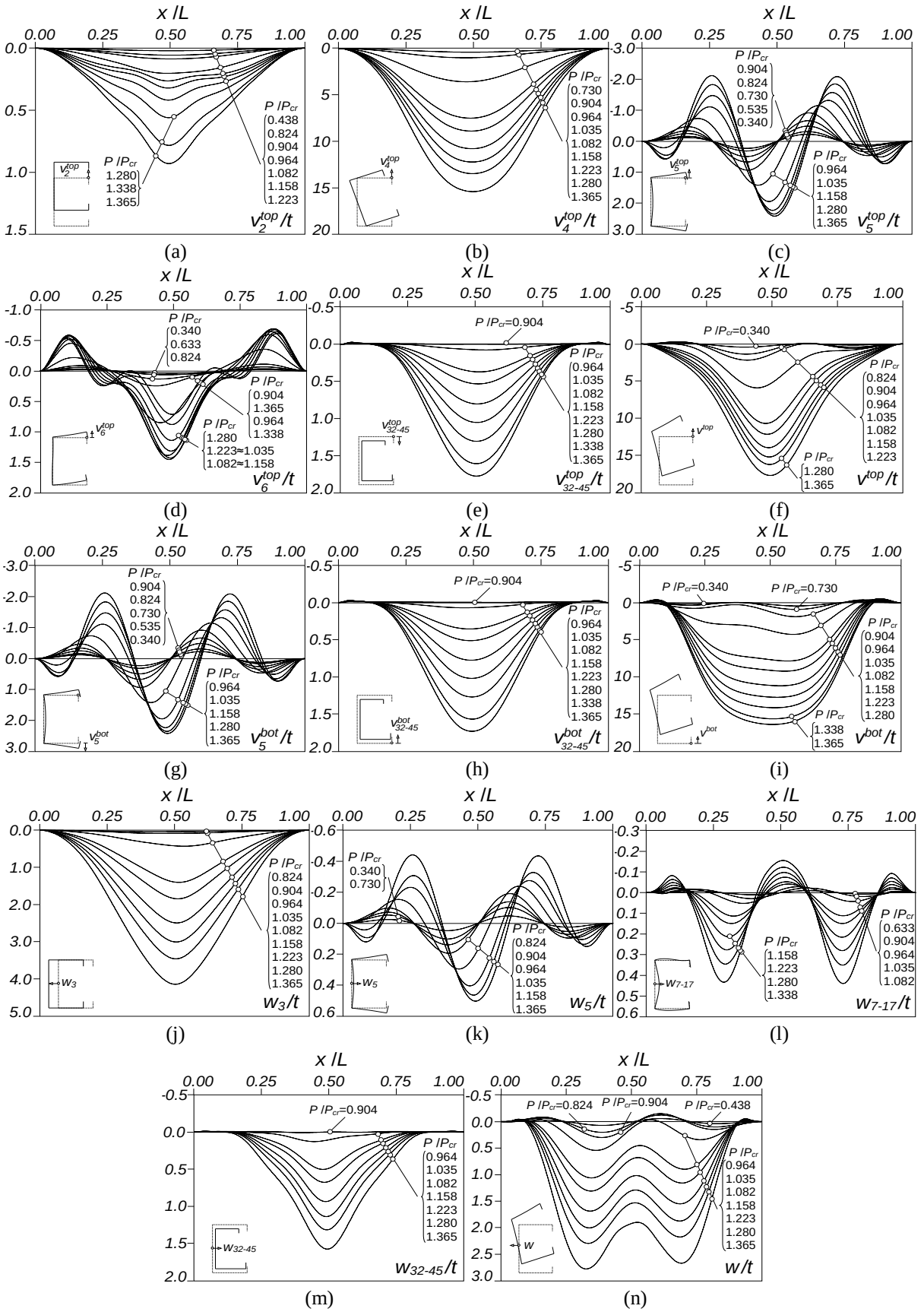

Figure 8: C_{DG}+{0.5G+0.5D} column displacement profiles: top flange-lip corner vertical displacement (a) v_2^{top}, (b) v_4^{top}, (c) v_5^{top}, (d) v_6^{top}, (e) $v_{32\text{-}45}^{top}$, (f) $v_{1\text{-}59}^{top} \equiv v^{top}$, bottom flange-lip corner vertical displacement (g) v_5^{bot}, (h) $v_{32\text{-}45}^{bot}$, (i) $v_{1\text{-}59}^{bot} \equiv v^{bot}$ and mid-web transverse displacement (j) w_3, (k) w_5, (l) $w_{7\text{-}17}$, (m) $w_{32\text{-}45}$, and (n) $w_{1\text{-}59} \equiv w$

shapes of the displacements profiles v_5^{top} and v_5^{bot} switch gradually from 4 half-waves (akin to the distortional critical buckling mode) to 5 half-waves (akin to the second distortional bucking mode), due to the longitudinal symmetry of the latter (favouring the interaction with the global buckling mode) – at P/P_{cr}=1.365, both v_5^{top} and v_5^{bot} are already perfectly symmetric. As a result of the above v_5^{top} and v_5^{bot} "shape switch", the displacement profiles v^{top}, v^{bot} and w exhibit an asymmetry that only vanishes completely at P/P_{cr}=1.365. At the advanced loading stages (P/P_{cr}=1.25 and P/P_{cr}=1.50), there is a high similarity between the displacement profiles and deformed configurations of the C_{DG}+G and C_{DG}+{0.5G+0.5D} columns (see Fig. 6(a_4)-(b_4), 6(a_5)-(b_5), 7(a)-(n) and 8(a)-(n)), which agrees with the fact that the corresponding equilibrium paths merge into a common curve (see Figs. 4(a)-(b)).

(vii) As shown in Figs. 7(b)+(f)+(i) and 8(b)+(f)+(i), the dominant contributions to v^{top} and v^{bot} come from mode **4**, a typical feature in column D-G interaction. Indeed, the v_2 values are about 10% of the v_4 ones during the whole loading range – see Figs. 5(a)-(b).

(viii) As shown in Fig. 7(j)-(n) and 8(j)-(n), the dominant contribution to w comes from mode **3**, which appears due to the effective centroid shift effects stemming from the substantial cross-section stress redistribution occurring at the advanced loading stages (due to distortional deformations).

(ix) The joint contribution of the local deformation modes (mostly mode **7**) to w is very small and stems from their participation in the first two distortional buckling modes, which explains why the number of local half-waves is always fairly small.

(x) The joint contribution of the linear transverse extension deformation modes (mostly mode **36** – global deviatoric) to v^{top}, v^{bot} and w is not negligible – in the last case, it significantly "opposes" the contribution from mode **3**, which explains the large difference between w_3 and w. It is worth noting that including the linear and quadratic transverse extension modes is absolutely essential to obtain accurate results (see Figs. 3(a)-(b)), even if the latter have virtually no impact on the displacement profiles – in the case of the linear modes such impact is restricted to the column central region (see Figs. 7(h)+(m) and 8(h)+(m)).

4.2.2 Column C_{DG}+D

The singular geometrically non-linear behaviour of column C_{DG}+D, containing pure distortional initial geometrical imperfections, is adresses in detail in this section[14]. Fig. 9 shows the evolution of the modal participations as loading progresses, while Figs. 10(a)-(h) display the evolution of the (i) top flange-lip corner vertical displacement profiles v_5^{top}, $v_{32\text{-}45}^{top}$ and $v_{1\text{-}59}^{top} \equiv v^{top}$, and (ii) mid-web transverse displacement profile w_3, w_5, $w_{7\text{-}17}$, $w_{32\text{-}45}$ and $w_{1\text{-}59} \equiv w$. Finally, Figs. 11(a_1)-(a_5) show column deformed configurations at P/P_{cr}={0.50; 0.75; 1.00; 1.25; 1.40} – the amplifications considered, for some of them, are given between brackets. The observation of these leads to the following conclusions:

(i) The modal participation diagram in Fig. 9 bears no resemblance with those of columns C_{DG}+G and C_{DG}+{0.5G+0.5D} (see Figs. 5(a)-(b)), thus evidencing this column singular behaviour, which is not affected by D-G interaction. Naturally, mode **1** governs at the early loading stages (p_1>60%), after which it is gradually replaced by modes **5** (mostly), **7** and **9** – the modes that contribute to the column initial geometrical imperfections (participations of 95%, 3%, 1%, respectively, which change very little during the early loading stages). As loading progresses, until $P/P_{cr}\approx$1.05, mode **3** emerges and its contribution gradually increases up to 14%, together with a similarly gradual growth of the participation of mode **5**, reaching a maximum of 56%. Beyond $P/P_{cr}\approx$1.05, the contributions of modes **3** and **5** part ways: the former further increases up to 33% at P/P_{cr}=1.40, while the latter reduces to 42%. As for the local mode contributions, they exhibit a smooth and small increase throughout the whole loading range, reaching 4.4% at P/P_{cr}=1.40 – modes **11** and **13** emerge at the advanced loading stages, but their contributions

[14] This behaviour has only theoretical interest, since is unlikely that a real column contains pure distortional initial geometrical imperfections.

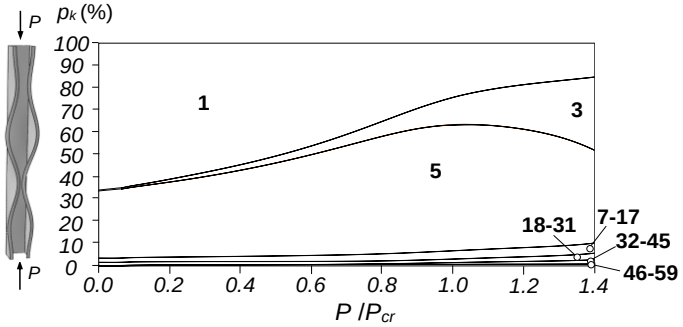

Figure 9: Modal participation diagram of the C_{DG}+D column

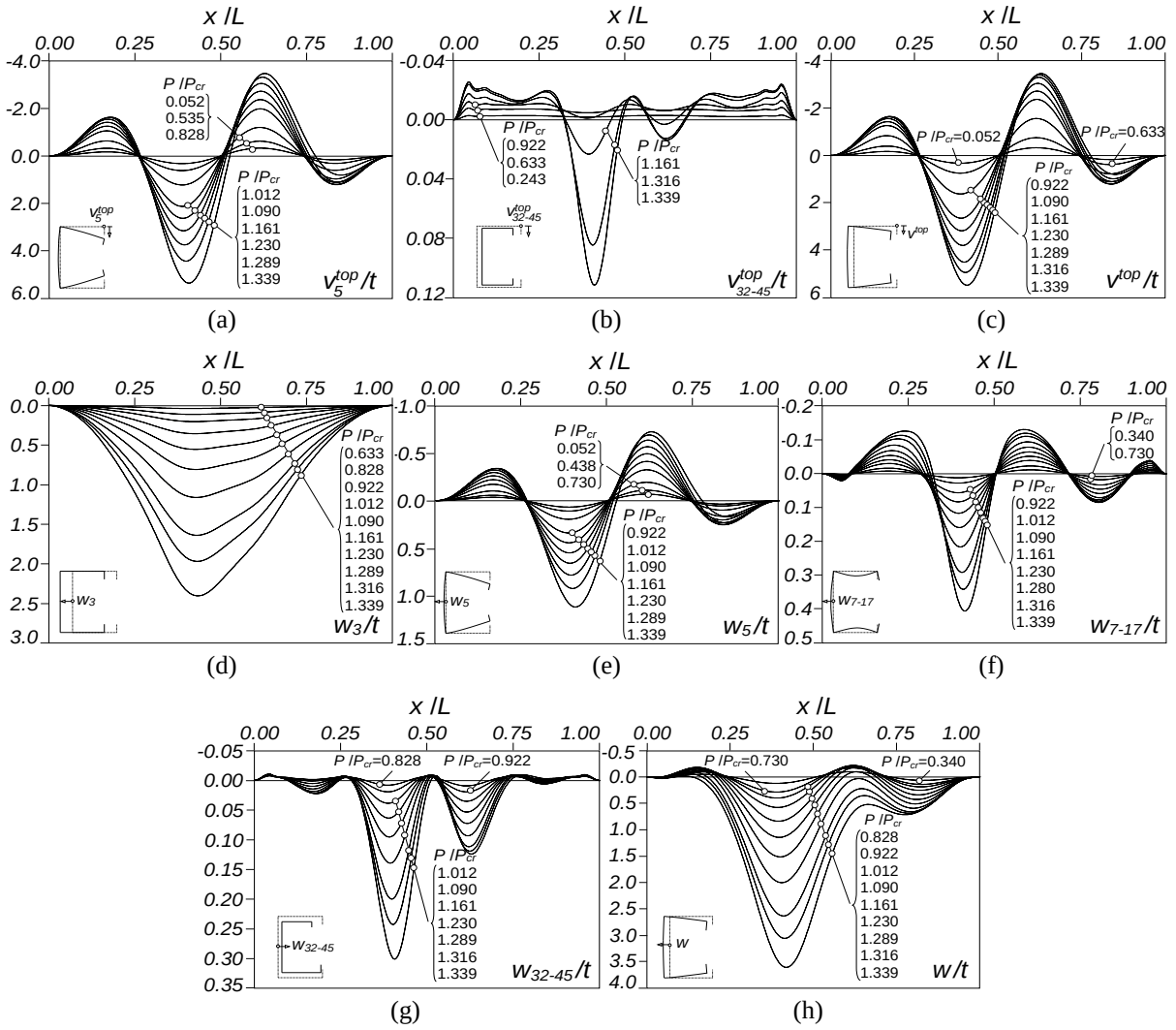

Figure 10: C_{DG}+D column displacement profiles: top flange-lip corner vertical displacement (a) v_5^{top}, (b) $v_{32\text{-}45}^{top}$, (c) $v_{1\text{-}59}^{top} \equiv v^{top}$, and mid-web transverse displacement (d) w_3, (e) w_5, (f) $w_{7\text{-}17}$, (g) $w_{32\text{-}45}$ and (h) $w_{1\text{-}59} \equiv w$

remain very tiny[15]. The shear modes (mostly mode **19**, but also modes **21**, **23**, **25** and **26**) emerge at $P/P_{cr} \approx 0.83$ – their joint participation reaches 2.2% at $P/P_{cr}=1.40$ (with $p_{19}=1.4\%$). Finally, the transverse extension modes **32** (mostly) and **35** are the most relevant for the column response, even if modes **34**, **38**-**42**, **44** and **45** also have minute contributions – their joint contribution never exceeds 4%, with $p_{32}=1.0\%$ and $p_{35}=0.8\%$.

[15] Since this column exhibits a symmetric deformed configuration (with respect to the cross-section major-axis), the anti-symmetric modes play no role in the structural response, unlike in the C_{DG}+G and C_{DG}+{0.5G+0.5D} columns, analysed earlier.

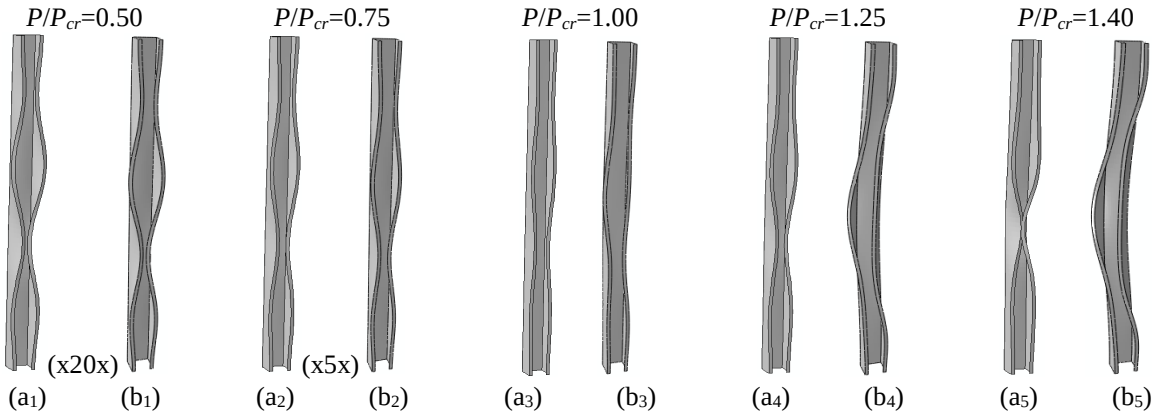

Figure 11: ABAQUS deformed configurations of the (a) C_{GD}+D (b) C_{GD}+{0.95D+0.05G} columns at loading stages defined by P/P_{cr} equal to ($_1$) 0.50, ($_2$) 0.75, ($_3$) 1.00, ($_4$)1.25 and ($_5$) 1.40

(ii) Figs. 10(a)-(c) show that the flange-lip corner vertical displacements profile (v^{top}) consists essentially of the contribution from mode **5** – the small difference between v^{top} and $v_5{}^{top}$ is due to the transverse extension modes (see Fig. 10(b)), which confirms that, indeed, this column is not affected by D-G interaction, despite the near coincidence of the distortional and "global" critical buckling loads. There are no contributions from modes **2**, **4** and **6** (those participating in the "global" critical buckling mode) – compare the deformed configurations shown in Figs. 11(a_1)-(a_5) and 6(a_1)-(b_5). In fact, the post-buckling behaviour of column response of this column resembles a typical distortional post-buckling behaviour (assertion that will be discussed after).

(iii) From Figs. 10(a)+(c) show that the shape of $v_5{}^{top}$ changes gradually from 4 equal half-waves (akin to the initial geometrical imperfection – *e.g.*, at P/P_{cr}=0.828) to unequal ones – the inner half-waves outgrow the outer ones (particularly that involving inward flange lip-motions).

(iv) The effective centroid shift caused by the stress redistribution due to the distortional deformations originates minor-axis bending, as shown in Fig. 10(d) – the w_3 and w_5 shapes are in accordance: asymmetric and with the higher values occurring to the left of the mid-span cross-section. Once more, the contribution of $w_{7\text{-}17}$ and $w_{32\text{-}45}$ to w is minute – w is practically the sum of w_3 and w_5.

In order to shed further light on the singular post-buckling behaviour exhibited by the C_{DG}+D column, the column characterised in Fig. 2(b), which has a critical distortional buckling load much lower than its local and global counterparts (*i.e.*, a pure distortional post-bucking behaviour), is analysed next. Because it was not possible to find a column buckling in a mode with 4 distortional half-waves not experiencing L-D interaction, the column selected buckles in a mode with 2 distortional half-waves. Two initial geometrical imperfections are considered, namely (i) pure distortional (C_D+D column) and (ii) pure global (C_D+G column)[16], making it possible to compare their post-buckling behaviours with those exhibited by of the C_{DG}+D and C_{DG}+G columns (addressed previously).

Fig. 12(a_1)-(a_2) show the equilibrium paths P/P_{crD} vs. $(v+v_0)/t$ of columns C_D+D and C_D+G, where v is the flange-lip corner vertical displacement at the location of the buckling mode most inward half-wave crest and at mid-span, respectively, normalised to an L/1000 amplitude – Figs. 12(b_1)-(b_2) provide the corresponding modal participation diagrams. Figs. 13(a)-(h) and 14(a)-(n) are similar to Figs. 10(a)-(h) and Fig. 7(a)-(n), respectively. Finally, Figs. 15(a_1)-(b_5) show C_D column deformed configurations at loading stages P/P_{cr}={0.50, 1.00, 1.25, 1.50, 1.75, 2.00} – the amplifications adopted are given inside brackets. The observation and comparison of the post-buckling results concerning the four columns under consideration makes it possible to draw the following conclusions:

[16] The initial geometrical imperfections used in the GNIA was obtained by solving an auxiliary buckling problem, either by (i) including only modes **2** and 4 (GBT analysis) or (ii) considering a higher wall thickness (SFEA), thus creating a column with the same mid-surface geometry that has a global critical buckling mode – see Fig. 12(a_2).

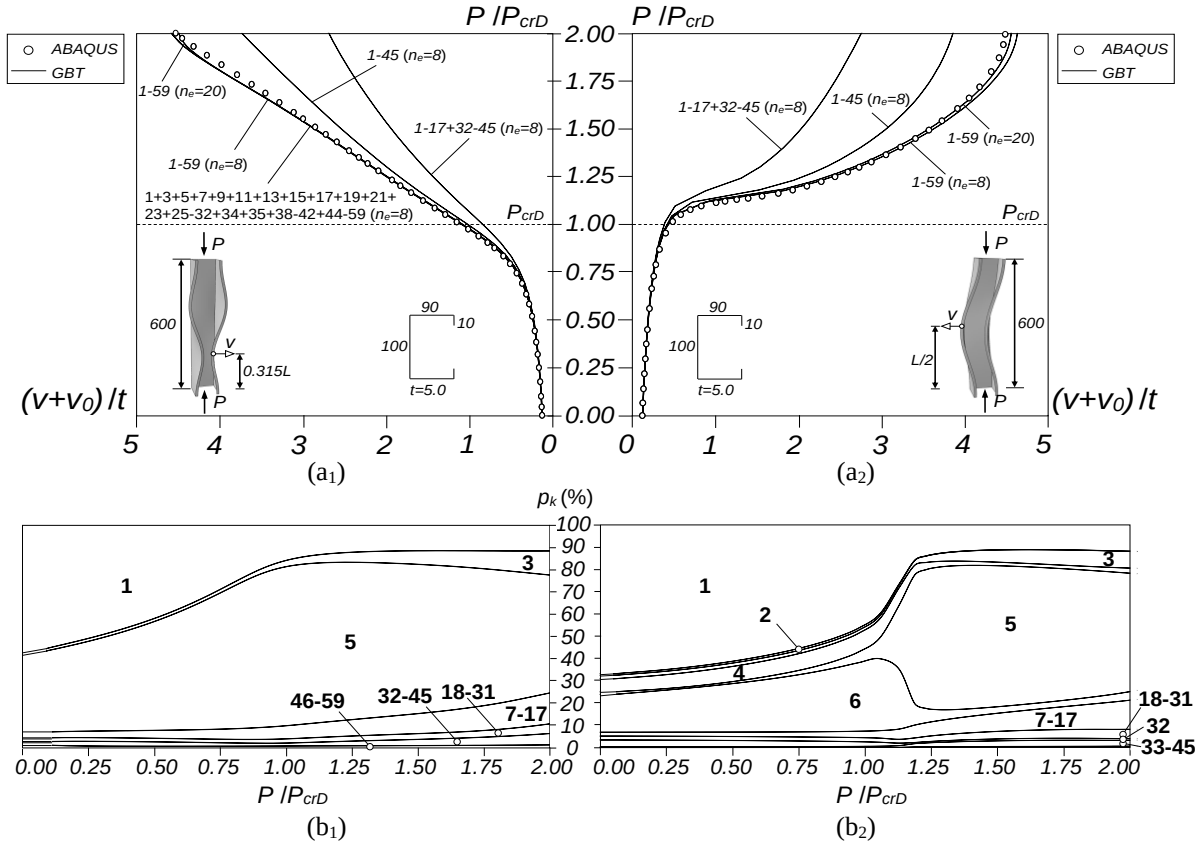

Figure 12: GBT (a) post-buckling equilibrium paths, for various discretisations (deformation mode sets and/or finite element numbers) and (b) modal amplitude diagrams of the (1) C_D+D and (2) C_D+G columns

(i) The SFEA validation procedure follows the same trends of that carried out for the C_{DG} columns (see Section 4.1) – the comments then made remain valid. The only difference is the inclusion, in Fig. 12(a_1), of the post-buckling equilibrium path obtained with the deformation mode set "**1**+**3**+**5**+**7**+**11**+**13**+**15**+**17**+**19**+**21**+**23**+**25-32**+**34**+**35**+**38-42**+**44-59**", which yields the same results as the inclusion of all modes (**1-59**) but with significantly less deformation modes.

(ii) Despite the different critical half-wave numbers of the C_{DG}+D and C_D+D columns (4 and 2), the joint observation of (ii$_1$) Fig. 12(b_1) (C_D+D) and Fig. 9 (C_{DG}+D), (ii$_2$) Fig. 13 (C_D+D) and Fig. 10 (C_{DG}+D), and (ii$_3$) Figs. 15(a_1)-(a_5) (C_D+D) and Fig. 11(a_1)-(a_5) (C_{DG}+D), shows a strong resemblance between their modal participation diagrams, displacements profiles and deformed configurations. Indeed, Figs. 10(a)-(c) and Figs. 13(a)-(c) share the same qualitative behaviour, *i.e.*, the displacement profile v^{top} (ii$_1$) almost coincides with v_5^{top} and (ii$_2$) exhibits initially 4 (C_{DG}+D) or 2 (C_D+D) equal half-waves that become gradually more unequal, with the largest deformations occurring in the central region and involving inward flange-lip motions. However, there is one main difference: the participation of mode **3** (w_3), which (ii$_1$) is more irregular in the C_{DG}+D column, mostly likely because of the higher critical mode half-wave number, and (ii$_2$) corresponds to higher p_3/p_5 ratios, at the advanced loading stages in the C_{DG}+D column, probably because the minor-axis flexural buckling load is closer and, therefore, provides more amplification to the deformation pattern associated with mode **3**.

(iii) The comparison between the post-buckling behaviours of the C_{DG}+D and C_D+D columns provides a clear explanation for the singularity the former: although the distortional and critical buckling loads are nearly coincident, it does not exhibit any trace of D-G interaction. Indeed, the post-buckling behaviours of the (iii$_1$) C_{DG}+D and (iii$_2$) C_{DG}+G and C_{DG}+{0.5D+0.5G} columns are clearly different, which implies that a "transition initial geometrical imperfection" must exist to separate them. Figs. 4(a)-(b) show also equilibrium paths of a C_{DG} column that

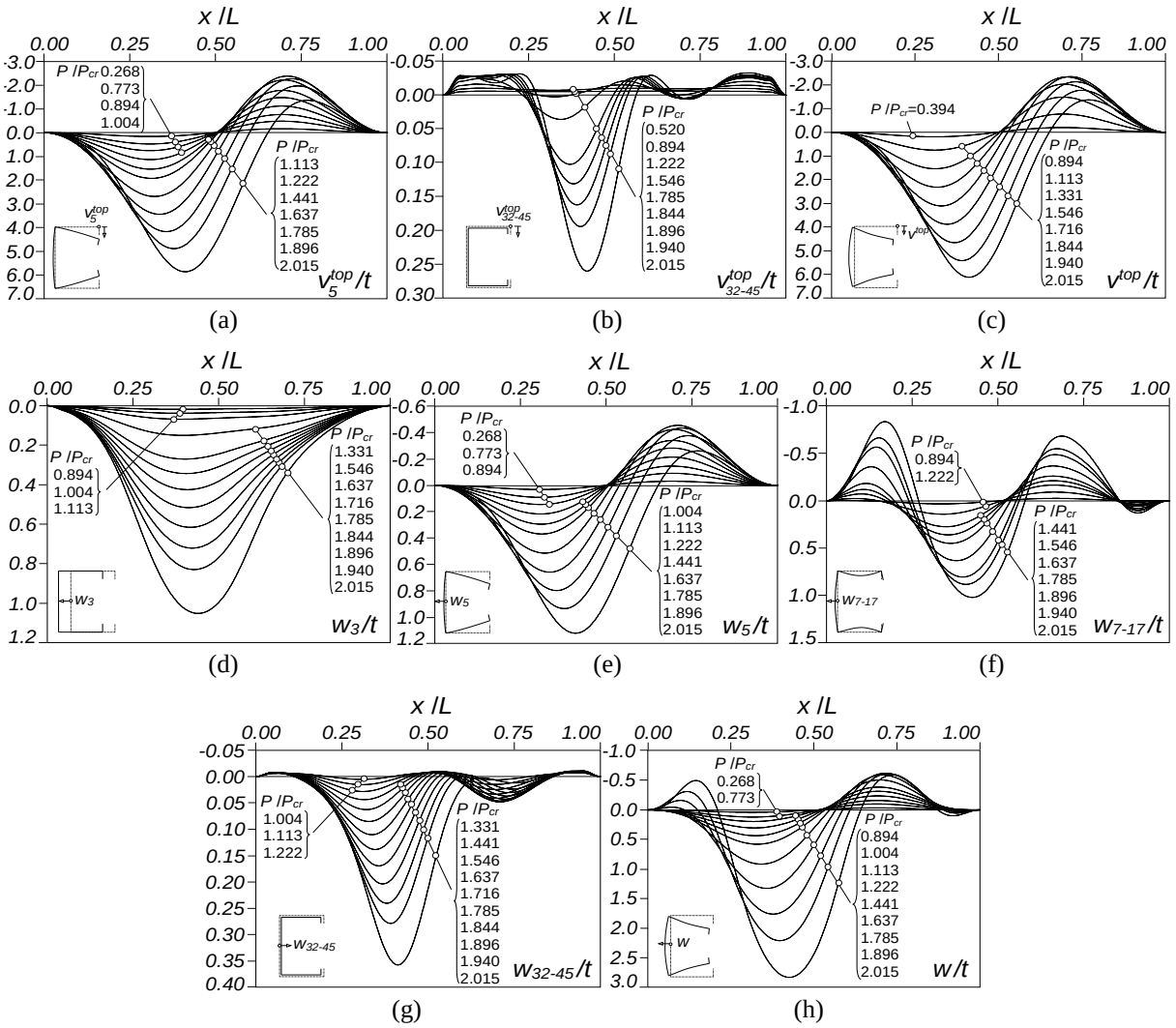

Figure 13: C_D+D column displacement profiles: top flange-lip corner vertical displacement (a) v_5^{top}, (b) $v_{32\text{-}45}^{top}$, (c) $v_{1\text{-}59}^{top} \equiv v^{top}$, and mid-web transverse displacement (d) w_3, (e) w_5, (f) $w_{7\text{-}17}$, (g) $w_{32\text{-}45}$, and (h) $w_{1\text{-}59} \equiv w$

contains an initial geometrical imperfection combining (iii_1) 95% of the distortional buckling mode with (iii_2) 5% of the global buckling mode, both normalised to $L/1000$ – column C_{DG}+{0.95D+0.05G}. On the other hand, Figs. 11(b_1)-(b_5) show deformed configurations of this column at P/P_{cr}={0.50, 0.75, 1.00, 1.25, 1.40}. As expected, these results show that column C_{DG}+{0.95D+0.05G} experiences true D-G interaction[17] (note the similarity between Figs. 11(b_1)-(b_5) and 6(a_1)-(b_5)) – therefore, it may be argued that the singular post-buckling behaviour exhibited by the C_{DG}+D column has only theoretical interest (no practical relevance).

(iv) The modal participation diagrams displayed in Figs. 12(b_1)-(b_2) are completely different for P/P_{crD}<1.25, due to the different nature of the initial geometrical imperfections. Fig. 12(b_2), concerning the C_D+G column, shows that mode **1** plays a dominant role in the early loading stages, after which it is quickly (and surprisingly) replaced by mode **6**, which reaches a peak participation of 32% at $P/P_{crD}\approx$1.05 – although the initial imperfection was purely global (modes **2**+**4**), the fact that the column "global" critical buckling mode includes also mode **6** explains its emergence. The participation of modes **2** and **4** remain practically constant until $P/P_{crD}\approx$1.05. Suddenly, at P/P_{crD}=1.05, the participation of mode **6** is drastically replaced by contributions from

[17] The displacements profiles are not shown because they are similar to those concerning column C_{DG}+{0.5D+0.5G} – only minor differences occur in the early loading stages. At advanced loading stages, the two column equilibrium paths merge into a common curve (Figs. 4(a)-(b)) and the deformed configurations combine 5 distortional half-waves with a dominant global (mostly torsional) half-wave.

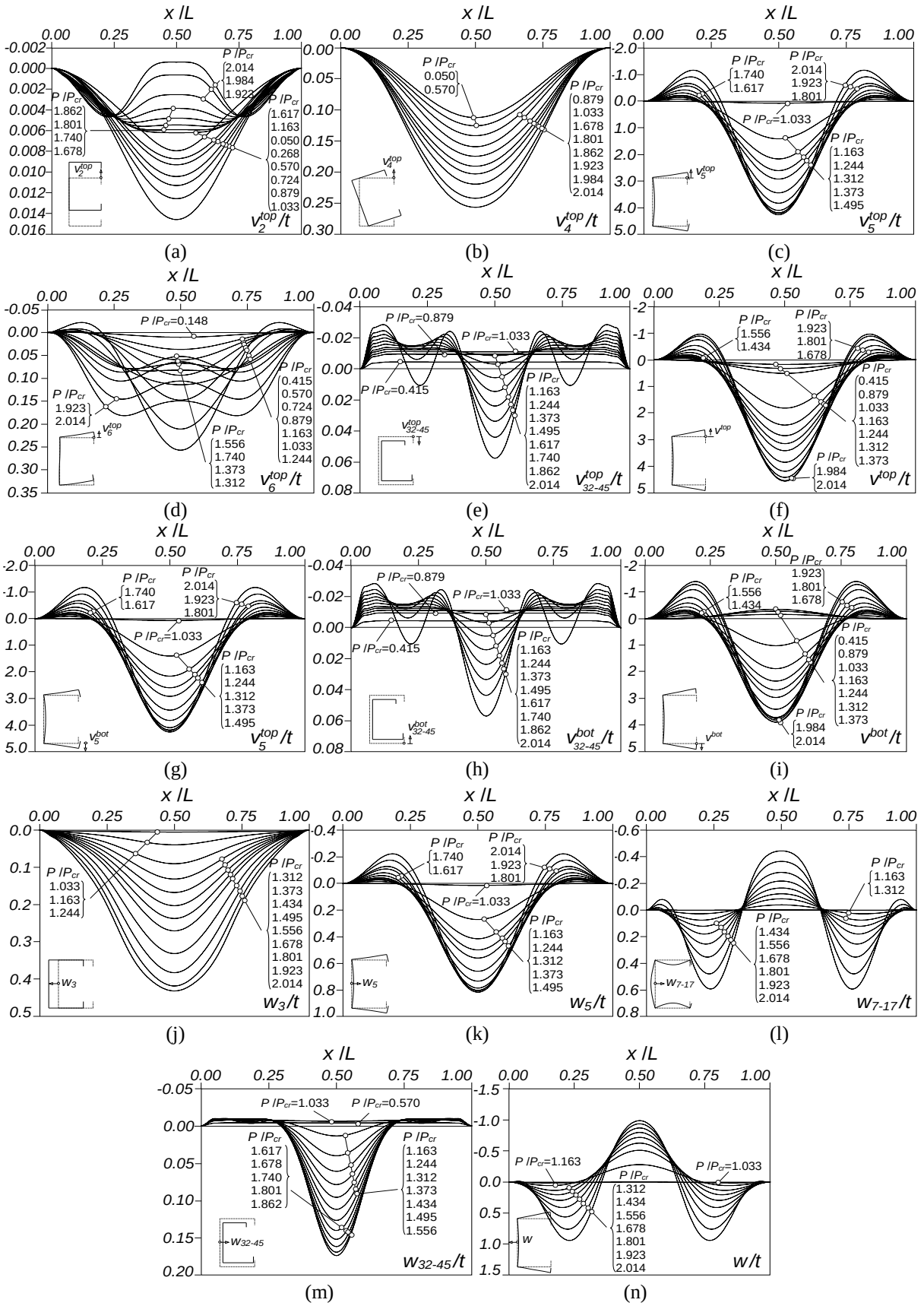

Figure 14: C_D+G column displacement profiles: top flange-lip corner vertical displacement (a) v_2^{top}, (b) v_4^{top}, (c) v_5^{top}, (d) v_6^{top}, (e) $v_{32\text{-}45}^{top}$, (f) $v_{1\text{-}59}^{top} \equiv v^{top}$, bottom flange-lip corner vertical displacement (g) v_5^{bot}, (h) $v_{32\text{-}45}^{bot}$, (i) $v_{1\text{-}59}^{bot} \equiv v^{bot}$ and mid-web transverse displacement (j) w_3, (k) w_5, (l) $w_{7\text{-}17}$, (m) $w_{32\text{-}45}$ and (n) $w_{1\text{-}59} \equiv w$

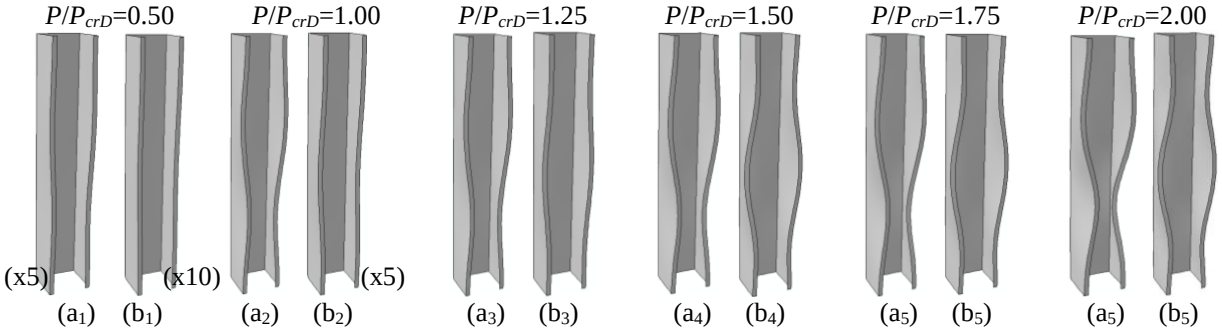

Figure 15: ABAQUS deformed configurations of at several C_D columns containing (a) distortional and (b) global initial geometrical imperfections for P/P_{crD} equal to (1) 0.50, (2) 1.00, (3) 1.25, (4) 1.50, (5) 1.75 and (6) 2.00

mode **5** (mostly), which emerges at $P/P_{crD}\approx0.74$ and increases smoothly, modes **7** and **9**, and mode **3**, which constitutes clear evidence of a distortional post-buckling behaviour. For higher loads, p_5 reaches a peak of 65% at $P/P_{crD}\approx1.37$, after which it is gradually replaced by increasingly relevant local, shear and transverse extension modes – their participations reach $p_{7\text{-}17}$=13%, $p_{18\text{-}31}$=4% and $p_{32\text{-}59}$=4% at P/P_{crD}=2.0. In qualitative terms, the participations of these modes, in the advanced loading stages, are similar in the C_D+G and C_D+D columns – the main differences are small participations from modes **6** and **4** (4% and 2% at P/P_{crD}=2.0).

(v) The results presented in Fig. 14(a)-(n) and Fig. 15(b_1)-(b_5), concerning the C_D+G column, provide further evidence on the singularity of the post-buckling behaviour of the C_{DG}+D column. Indeed, as expected, the global initial imperfection does not cause D-G interaction. Nevertheless, there are differences between the C_D+D and C_D+G column post-buckling behaviours that are not reflected in their modal participations diagrams and should be pointed out:

(v.1) The C_D+G column post-buckling behaviour involves mainly the participation of three distortional half-waves. The critical buckling mode two half-waves combine with the three half-waves of the second buckling mode, which becomes progressively dominant – this is due to the 8% difference between the associated buckling loads (1158.5kN vs. 1258.4kN). Thus, the displacement profiles w_3 (Fig. 14(j)), $w_{7\text{-}17}$ (Fig. 14(l)), $v_{32\text{-}45}$ and $w_{32\text{-}45}$ (Figs. 14(e)+(m)) change accordingly.

(v.2) The C_D+D column post-buckling behaviour has no contributions from modes **2**, **4** and **6**, while the C_D+D column one contains only small contributions from modes **2** (Fig. 14(a)) and, mostly, **4** (Fig. 14(b)), which were included in the initial geometrical imperfection – mode **6** (Fig. 15(d)), excluded from the initial geometrical imperfection, emerges only at a later stage and is responsible for the difference between v^{top} and v^{bot} (Figs. 14(f)+(i)).

5 CONCLUSION

A GBT-based investigation on the geometrically non-linear elastic post-buckling behaviour of fixed-ended lipped channel columns undergoing D-G interaction was reported. The results presented and discussed were validated through the comparison with ABAQUS SFEA values and shed new light on the mechanics underlying the structural behaviour associated with this coupling phenomenon. They consisted of equilibrium paths and plots providing the evolution, along such paths, of (i) GBT-based displacement profiles and modal participation diagrams, and (ii) ABAQUS deformed configurations.

After a brief review of the GBT elastic non-linear formulation, GBT buckling analyses were employed to obtain geometries of columns experiencing (i) D-G interaction and (ii) a pure distortional post-bucking behaviour. Next, the GBT GNIA equilibrium paths results, concerning columns with initial geometrical imperfections having amplitude L/1000 and combining differently the critical distortional and global buckling modes, were validated through the comparison with ABAQUS SFEA

values. Finally, GBT GNIA results concerning several lipped channel columns were presented and discussed, with the aim of acquiring fresh insight on the mechanics underlying D-G interaction. Among the various findings unveiled in this investigation, the following ones deserve to be specially mentioned:

(i) The so-called global critical buckling mode has contributions from torsion, major-axis flexure and anti-symmetric distortion (modes **2**, **4** and **6**). As for the distortional critical buckling mode, it has small participations from local modes (**7** and **9**).

(ii) The equilibrium path of a column with nearly coincident critical distortional and global buckling loads depends significantly on the shape of the initial geometrical imperfection, namely on whether it is pure distortional or not (*i.e.*, contains a global component, regardless of how small) – D-G interaction only occurs in the latter case.

(iii) The deformed configurations of the columns undergoing D-G interaction exhibit, in the advanced loading stages, are predominantly global, mostly due to torsional deformations – the contribution of major-axis flexure is small and minor-axis flexure only appears when the effective centroid shift effects caused by the stress redistribution (due to the symmetrical distortional deformations – mode **5**) become important. The anti-symmetric deformations are only relevant in the earlier loading stages – they fade away as loading progresses.

(iv) Although the different initial geometrical imperfections entail non-negligible differences in the earlier loading stages, the post-buckling behaviours of the C_{DG}+G and C_{DG}+{0.5G+0.5D} are quite similar, both characterised by the occurrence of significant D-G interaction. As mentioned above, and quite surprisingly, the C_{DG}+D column post-buckling behaviour is not affected by D-G interaction, despite the nearly coincidence between the two competing critical buckling loads – no such behavioural feature was ever observed in the context of column L-D or L-D-G interaction.

(v) The comparison between the post-buckling behaviours of C_{DG} and C_D columns (the latter exhibit a pure distortional post-buckling behaviour) showed that may be very similar or very different, depending on whether the initial geometrical imperfection is distortional and global, thus confirming that D-G interaction does not occur in the C_{DG} column in the presence of pure distortional initial imperfections – an unexpected singular post-buckling behaviour.

(vi) The next step of this numerical ongoing investigation is to assess the ultimate strength erosion caused by D-G interaction in elastic-plastic cold-formed steel columns, a very important issue as far as the design of such columns is concerned.

ACKNOWLEDGEMENTS

The first author gratefully acknowledges the financial support of FCT (*Fundação para a Ciência e a Tecnologia* – Portugal) through the doctoral scholarship SFRH/BD/87746/2012.

REFERENCES

[1] Camotim D. and Dinis P.B., "Coupled instabilities with distortional buckling in cold-formed steel lipped channel columns", *Thin-Walled Structures*, **49**(5), 562-575, 2011.

[2] Kwon Y.B. and Hancock G.J., "Tests of cold-formed channels with local and distortional buckling", *Journal of Structural Engineering* (ASCE), **118**(7), 1786-1803, 1992.

[3] Young B., Silvestre N. and Camotim D., "Cold-formed steel lipped channel columns influenced by local-distortional interaction: strength and DSM design", *Journal of Structural Engineering* (ASCE), **139**(6), 1059-1074, 2013.

[4] Martins A.D., Dinis P.B., Camotim D. and Providência P., "On the relevance of local-distortional interaction effects in the behaviour and design of cold-formed steel columns", *Computers & Structures*, **160**(November), 57-89, 2015.

[5] Martins A.D., Dinis P.B. and Camotim D., "On the influence of local-distortional interaction in the behaviour and design of cold-formed steel web-stiffened lipped channel columns", *Thin-Walled Structures*, **101**(April), 181-204, 2016.

[6] Martins A.D., Camotim D. and Dinis P.B., "On the direct strength design of cold-formed steel columns failing in local-distortional interactive modes", *Proceedings of Wei-Wen Yu International Specialty Conference on Cold-Formed Steel Structures* (Baltimore, 9-10/09), 2016. (in press)

[7] Crisan A., Ungureanu V. and Dubina D., "Behaviour of cold-formed steel perforated sections in compression – part 1: experimental investigations", *Thin-Walled Structures*, **61**(December), 86-96, 2012.

[8] Dubina D., Ungureanu V. and Crisan A., "Experimental evidence of erosion of critical load in interactive buckling", *Journal of Structural Engineering* (ASCE), **139**(5), 705-716, 2013.

[9] Santos E.S., Batista E.M. and Camotim D., "Experimental investigation concerning lipped channel columns undergoing local-distortional-global buckling mode interaction", *Thin-Walled Structures*, **54**(May), 19-34, 2012.

[10] Anbarasu M. and Murugapandian G., "Experimental study on cold-formed steel web stiffened lipped channel columns undergoing distortional-global interaction", *Material & Structures*, **49**(4), 1433-42, 2016.

[11] Rossi B., Jaspart J.-P. and Rasmussen K.J.R., "Combined distortional and overall flexural-torsional buckling of cold-formed stainless steel sections: experimental investigations", *Journal of Structural Engineering* (ASCE), **136**(4), 354-360, 2010.

[12] Rossi B., Jaspart J.-P. and Rasmussen K.J.R., "Combined distortional and overall flexural-torsional buckling of cold-formed stainless steel sections: design", *Journal of Structural Engineering* (ASCE), **136**(4), 361-369, 2010.

[13] Dinis P.B. and Camotim D., "Post-buckling behaviour and strength of cold-formed steel lipped channel columns experiencing distortional/global interaction", *Computers & Structures*, **89**(3-4), February, 422-434, 2011.

[14] Camotim D. and Dinis P.B., "Distortional/global interaction in lipped channel columns", *Proceedings of the Institution of Civil Engineers (ICE)-Structures and Buildings*, **166**(8), 381-391, 2013.

[15] Crisan A., Ungureanu V. and Dubina D., "Behaviour of cold-formed steel perforated sections in compression – Part 2: numerical investigations and design considerations", *Thin-Walled Structures*, **61**(December), 97-105, 2012.

[16] Camotim D., Silvestre N., Gonçalves R., Dinis P.B., "GBT analysis of thin-walled members: new formulations and applications, *Thin-Walled Structures: Recent Advances and Future Trends in Thin-Walled Structures Technology*, J. Loughlan (ed.), Canopus Publishing Ltd. (Bath), 137-168, 2004.

[17] Simulia Inc., *ABAQUS Standard* (version 6.7-5), 2008.

[18] Martins A.D., Camotim D., Gonçalves R. and Dinis P.B., "On the mechanics of local-distortional interaction in thin-walled lipped channel beams", *Proceedings of 7th International Conference on Coupled Instabilities in Metal Structures*, (CIMS 2016 – Baltimore, 7-8/11), 2016. (in press)

[19] Gonçalves R. and Camotim D., "Geometrically non-linear generalized beam theory for elastoplastic thin-walled metal members", *Thin-Walled Structures*, **51**(February), 121-129, 2012.

[20] Kwon Y.B. and Hancock G.J., "Post-buckling analysis of thin-walled channel sections undergoing local and distortional buckling", *Computers & Structures*, **49**(3), 507-516, 1993.

[21] Crisfield M.A., *Non-Linear Finite Element Analysis of Solids and Structures* (Volume 1: *Essentials*). John Wiley & Sons Ltd (Chichester), 2001.

[22] Ritto-Corrêa M. and Camotim D., "On the arc-length and other quadratic control methods: established, less known and new implementation procedures", *Computers & Structures*, **86**(11-12), 1353-1368, 2008.

[23] Gonçalves R., Bebiano R. and Camotim, D., "On the shear deformation modes in the framework of generalized beam theory", *Thin-Walled Structures*, **84**(November), 325-334, 2014.

[24] Bebiano R., Gonçalves R. and Camotim D., "A cross-section analysis procedure to rationalise and automate the performance of GBT-based structural analysis", *Thin-Walled Structures*, **92**(July), 29-47, 2015.

[25] Bebiano R., Camotim D. and Gonçalves R., "GBTUL 2.0 – a second-generation code for the GBT-based buckling and vibration analysis of thin-walled members", *submitted for publication*, 2016.

[26] Abambres M., Camotim D. and Silvestre N., "Modal decomposition of thin-walled member collapse mechanisms", *Thin-Walled Structures*, **74**(January), 269-291, 2014.

[27] Silvestre N. and Camotim D., "Local-plate and distortional postbuckling behavior of cold-formed steel lipped channel columns with intermediate stiffeners", *Journal of Structural Engineering* (ASCE), **132**(4), 529-540, 2006.